Volume 57
Number 16
25 February 2021
Pages 1965–2100

ChemComm

Chemical Communications

rsc.li/chemcomm

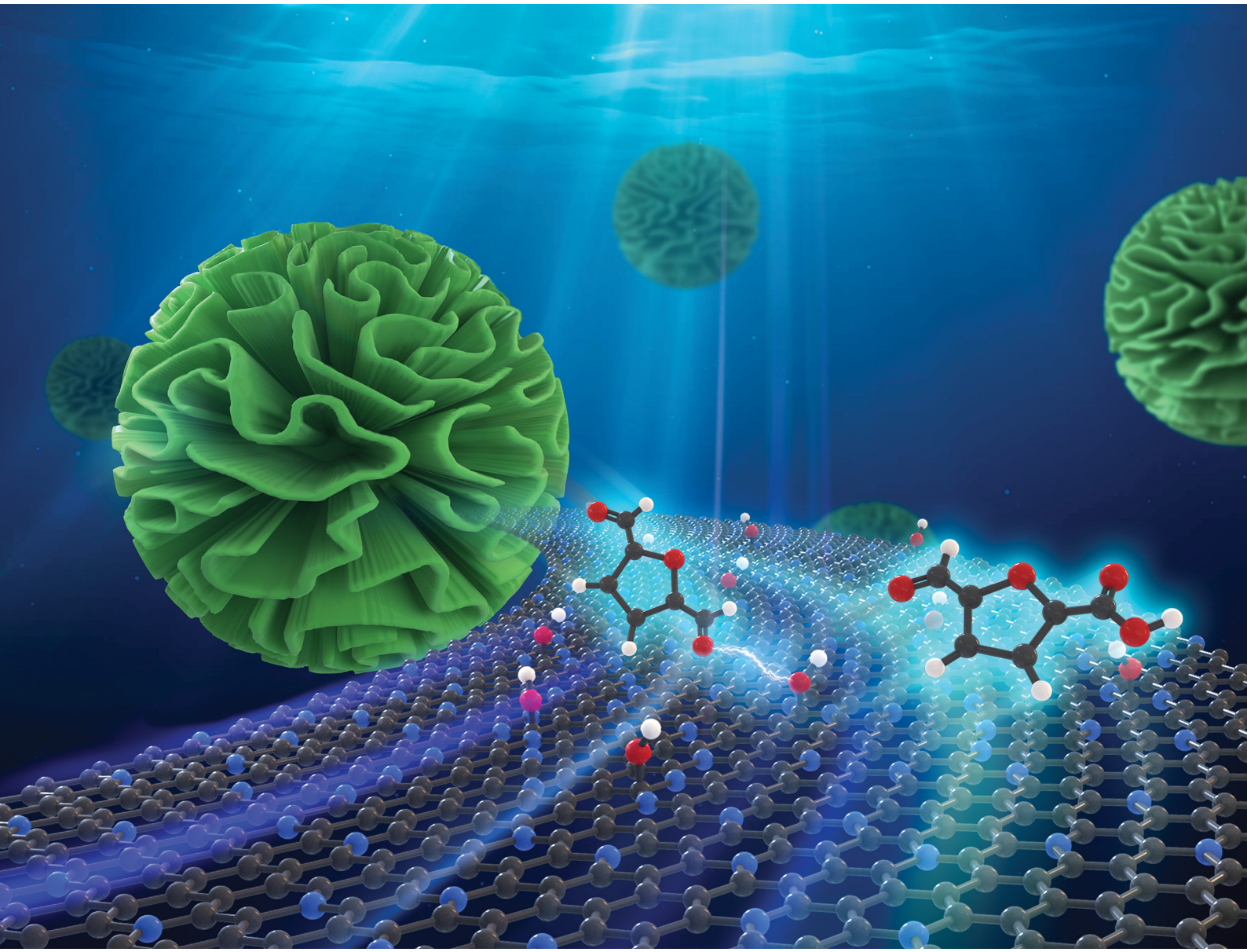

ISSN 1359-7345

ROYAL SOCIETY OF CHEMISTRY

COMMUNICATION

Vivek Polshettiwar, Hua Tan *et al.*

Nitrogen doped carbon spheres with wrinkled cages for the selective oxidation of 5-hydroxymethylfurfural to 5-formyl-2-furancarboxylic acid

ChemComm

COMMUNICATION

View Article Online
View Journal | View Issue

Cite this: *Chem. Commun.*, 2021, **57**, 2005

Received 2nd December 2020,
Accepted 21st January 2021

DOI: 10.1039/d0cc07856e

rsc.li/chemcomm

Nitrogen doped carbon spheres with wrinkled cages for the selective oxidation of 5-hydroxymethylfurfural to 5-formyl-2-furancarboxylic acid†

Jiaping Zhu,[a] Chaojian Yao,[a] Ayan Maity,[b] Jielai Xu,[a] Tong Zhan,[cd] Weibing Liu,[a] Mingtai Sun,[c] Suhua Wang,[c] Vivek Polshettiwar *[b] and Hua Tan *[a]

Nitrogen doped carbon spheres with wrinkled cages (NCSWCs), which were used for the first time as metal-free catalysts, exhibited high catalytic activity and selectivity in the oxidation of 5-hydroxymethylfurfural (HMF) to 5-formyl-2-furancarboxylic acid (FFCA) under base-free conditions using *tert*-butyl hydroperoxide (TBHP) as the oxidant. The mechanistic studies found that this reaction was catalyzed by the synergy between NCSWCs and TBHP. The density functional theory (DFT) calculations further suggested that the hydroperoxyl radicals from TBHP adsorbed on the carbon atoms adjacent to the graphitic N atoms are the active sites.

HMF, as one of the important platform chemicals, can be oxidized to a series of value-added chemicals, such as 2,5-diformylfuran (DFF), 5-hydroxymethyl-2-furancarboxylic acid (HMFCA), FFCA, 2,5-furancarboxylic acid (FDCA), *etc.*[1] However, most studies were focused on the selective oxidation of HMF to DFF or FDCA due to their versatility as monomers and intermediates for pharmaceuticals, ligands, and other applications.[2,3] FFCA, which has promising applications in fuels, chemical intermediates, and drugs, *etc.*, has not yet received widespread attention, although several studies have been reported on the production of FFCA by the oxidation of HMF over metal based catalysts.[4–8]

Recently, considering the economic cost and environmental friendliness, N-doped carbon materials (NCs) have been widely used as metal-free catalysts for various chemical reactions, including HMF oxidation to DFF or FDCA.[9–15] The doped nitrogen atoms can modulate the surface properties of the carbon materials and also improve their electronic features, which thus leads to the enhancement of their catalytic performance as metal-free catalysts. On the other hand, N-doped hollow porous carbon spheres (NHCSs), which contain a combined micro/mesoporous shell and macroporous cage, have drawn more and more research interest in supercapacitors and rechargeable batteries.[16,17] However, NHCSs have been seldom used as metal-free catalysts for organic catalytic reactions in the literature.

NHCSs are synthesized using the hard templating method, soft templating method, modified Stöber method, hydrothermal carbonization method, and so on.[16] Among these methods, the hard templating method is more facile and controllable. The only drawback for this method is poor availability of the hard templates with tunable size, shape, and morphology.[18] Dendritic fibrous nanosilica (DFNS) possesses special fibrous morphology, which leads to high surface area and enhanced accessibility compared with mesoporous silica and can be synthesized on a large scale and their sizes, surface areas, and fiber densities can be controlled.[19,20] Thus, in this work, DFNS was used as the hard template to synthesize NCSWCs first *via* the hydrothermal carbonization using glucose as the carbon source, and then pyrolysis with 5,5′-diamino-3,3′-bis(1*H*-1,2,4-triazole) (DABT) as the nitrogen source, followed by template etching. The obtained NCSWCs were used as metal-free catalysts in the oxidation of HMF to FFAC under base-free conditions.

The DFNS used in the synthesis are DFNS-1, 2, 3, and 4, which have different sphere sizes and fibrous morphologies with varying fiber densities, as shown in Fig. S1 (ESI†). Their adsorption and desorption isotherms in Fig. S2 (ESI†) indicated that DFNS is a typical mesoporous material and its detailed textural properties are summarized in Table S1 (ESI†). The TEM images of the obtained NCSWCs shown in Fig. 1(a–d) and Fig. S3 (ESI†) indicated that the sizes of NCSWC-1-800, NCSWC-2-800, NCSWC-3-800, or NCSWC-4-800 are similar to

[a] *College of Chemistry, Guangdong University of Petrochemical Technology, Maoming 525000, P. R. China. E-mail: huatan@gdupt.edu.cn*
[b] *Department of Chemical Sciences, Tata Institute of Fundamental Research (TIFR), Dr Homi Bhabha Road, Mumbai-400005, India. E-mail: vivekpol@tifr.res.in*
[c] *College of Environmental Science and Engineering, Guangdong University of Petrochemical Technology, Maoming 525000, P. R. China*
[d] *Guangdong Provincial Key Laboratory of Petrochemical Pollution Process and Control, Maoming 525000, P. R. China*

† Electronic supplementary information (ESI) available: Experimental, TEM, N_2 sorption isotherms, textural properties and chemical compositions, the relationship between catalytic activity and different N species, XRD, Raman, XPS N 1s spectra, and catalytic stability tests. See DOI: 10.1039/d0cc07856e

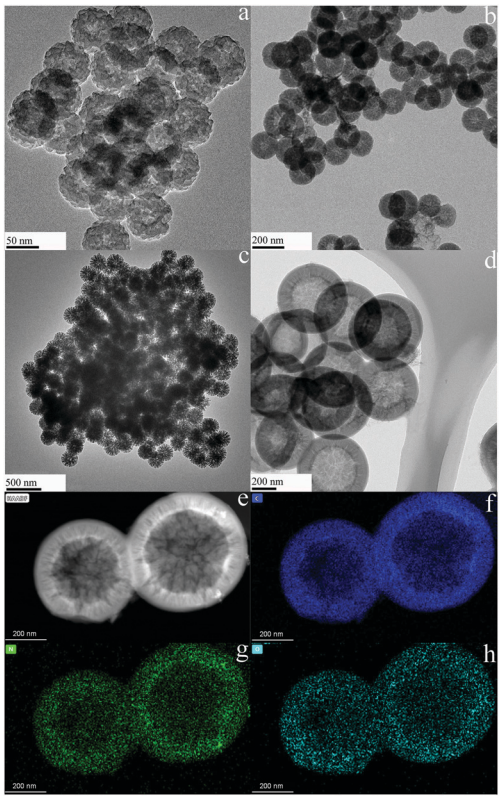

Fig. 1 TEM images of NCSWC-1-800 (a), NCSWC-2-800 (b), NCSWC-3-800 (c), and NCSWC-4-800 (d) and EDX mapping for C (f), N (g) and O (h) of the STEM image (e) of NCSWC-4-800.

those of the corresponding DFNS and the diameters of their cages were approximately 20–30 nm, 40–50 nm, 40–50 nm, and 300–350 nm, respectively. Moreover, different morphologies of the wrinkled cages in NCSWCs-800 suggested that the carbon precursor can be diffused well within the inner part of DFNS. These results demonstrated that this synthetic method allowed the preparation of NCSWCs with different sphere/cage sizes and morphologies of the wrinkled cages by using DFNS with different size and fiber density as the hard template, which normally cannot be achieved by using the solid spheres of silica.

All the NCSWCs-800 exhibits a typical IV-type curve with a hysteresis loop and a steep uptake (P/P_0 >0.97) in Fig. S4 (ESI†), indicating the coexistence of mesopores and macropores. The detailed textural parameters of the NCSWCs-800 in Table S2 (ESI†) show that the BET surface areas of NCSWCs-800 are in the range from 742.4 $cm^2\ g^{-1}$ to 965.6 $cm^2\ g^{-1}$, and notably, NCSWC-4-800 possessed the largest mesopore and macropore volumes among all the NCSWCs-800, which are probably derived from its huge wrinkled cages. The Barrett–Joyner–Halenda (BJH) pore size distributions in Fig. S4 (ESI†) show that NCSWCs-800, like DFNS, also contains dual pores, small and narrow pores, whose sizes are located at 2–3.5 nm, and the large and broad pores, whose sizes are larger than 10 nm. The XRD patterns of NCSWCs in Fig. S6 (ESI†) show two peaks at around 24.6° and 43.7°, which are attributed to the (002) and (100) planes of graphite, respectively. The intensity of the (002) peak increased with the increase of the pyrolysis temperature from 600 °C to 950 °C, which suggests that the content of graphitic carbon increased from NCSWC-4-600, to NCSWC-4-800, and then to NCSWC-4-950. The Raman spectra in Fig. S7 (ESI†) show that the NCSWCs exhibited two strong peaks at 1588 cm^{-1} (G band) and 1349 cm^{-1} (D band). The intensity ratio of I_D/I_G reduced as the pyrolysis temperature increased, suggesting an improved crystalline structure in NCSWCs with fewer defect sites as the pyrolysis temperature rises.

Elemental analysis on NCSWCs-800 listed in Table S2 (ESI†) confirms that the N contents in NCSWC-1-800, NCSWC-2-800, NCSWC-3-800, and NCSWC-4-800 are 13.69 wt%, 16.34 wt%, 14.92 wt%, and 15.21 wt%, respectively. The STEM-EDX elemental mapping results in Fig. 1(f–h) also reveal that the element N is homogenously distributed in the whole NCSWC-4-800. We also prepared NCSWC by pyrolysis with melamine at 600 °C and 800 °C for comparison, which were designated as NCSWC-4-600-M and NCSWC-4-800-M, respectively.[21] It can be seen from Table S2 (ESI†) that the N contents are 17.09 wt% and 7.12 wt% in NCSWC-4-600-M and NCSWC-4-800-M, respectively, while the N contents can reach up to 26.18 wt% and 15.21 wt% in NCSWC-4-600 and NCSWC-4-800, respectively, and even when the pyrolysis temperature reached 950 °C, 6.77 wt% of N content can be still retained in NCSWC-4-950. In addition, compared with NCs prepared by the post treatment method with urea or NH_3 as the nitrogen sources, the N contents in the NCSWCs are also much higher.[9,22]

XPS quantitative analysis also indicates that N with high contents exists in NCSWCs-800, as shown in Table S2 (ESI†). Their high resolution XPS N 1s spectra in Fig. S8 (ESI†) can be curve-fitted into three components located at around 398.6 ± 0.1 eV, 400.1 ± 0.1 eV, and 401.1 ± 0.1 eV, which correspond to pyridinic N, pyrrolic N, and graphitic N, respectively.[23] The relative peak areas of different N species are listed in Table S3 (ESI†). When the pyrolysis temperature is 600 °C, the most abundant N species is pyridinic N in NCSWC-4-600, whose relative peak area is 56.43%, with the increase of the pyrolysis temperature, the relative peak areas of pyridinic N and pyrrolic N decrease, but that of graphitic N rapidly increases from 9.84% to 42.32% in NCSWC-4-800, and then to 51.98% in NCSWC-4-950, respectively. As for NCSWCs-4-M, the relative peak areas of graphitic N are only 14.94% and 20.64% in NCSWC-4-600-M and NCSWC-4-800-M, respectively. Besides, the contents of graphitic N and pyridinic N are also listed in Table S3 (ESI†).

The catalytic performance of NCSWCs-800 was evaluated in HMF oxidation using TBHP as the oxidant under base-free conditions. It can be seen from Table 1 that FFCA was produced as the main product on all the NCSWCs-800 with high selectivity (~90%), but HMF conversion varied on different NCSWCs, from the lowest 79.1% on NCSWC-1-800, to 85.4% on NCSWC-3-800, 86.7% on NCSWC-2-800, and to the highest of 92.3% on NCSWC-4-800. Combined with the characterization results, the highest catalytic activity of NCSWC-4-800 could be attributed to its largest mesopore and macropore volumes. To examine the roles of NCSWCs-800 and TBHP in this reaction, HMF oxidation was

Table 1 Catalytic activity of various catalysts in HMF oxidation

Samples	HMF Conv. (%)	Selectivity (%)				FFCA yield (%)
		DFF	HMFCA	FFCA	FDCA	
NCSWC-1-800	79.1	8.3	1.1	89.2	1.1	70.6
NCSWC-2-800	86.7	7.2	1.2	90.1	1.2	78.1
NCSWC-3-800	85.4	7.9	1.6	88.6	1.5	75.7
NCSWC-4-800	92.3	5.8	1.4	90.5	1.9	83.5
NCSWC-4-600	67.2	22.1	1.4	74.7	0.9	50.2
NCSWC-4-950	75.7	13.1	1.1	83.3	1.6	63.1
NCSWC-4-800-M	62.5	29.6	1.0	67.3	1.3	42.1
NMC-800	58.6	35.5	1.7	61.8	0	36.2
No catalyst	32.3	7.2	0	0	0	0
NCSWC-4-800[a]	38.7	88.7	2.1	8.6	0	3.3

Reaction conditions: 10 mL HMF aqueous solution (0.05 mol L^{-1}), 50 mg catalyst, 70 wt% TBHP aqueous solution (TBHP/HMF = 4, molar ratio), reaction temperature = 100 °C, reaction time = 8 h. [a] 1 MPa O_2 instead of TBHP.

first conducted using TBHP as the oxidant without catalysts, the HMF conversion can reach 32.3%, but only DFF as the desired oxidation product with very low selectivity (7.2%) was obtained, as shown in Table 1. HMF oxidation was also conducted by using 1 MPa O_2 to replace TBHP over NCSWC-4-800, and 38.7% HMF conversion can also be achieved, with DFF, as the main product, as well as the other desired HMF oxidation products, such as HMFCA, and FFCA, obtained without producing any degradation products. Furthermore, if TBHP was added in this reaction with the TBHP/HMF molar ratio of 2, the HMF conversion was increased to 65.9% and FFCA became the main product with the yield of 38.5%. When the TBHP/HMF molar ratio reached 6, although full HMF conversion can be achieved, the FFCA yield is only 73.4%, because degradation products were produced. These results suggested that the HMF oxidation to FFCA in this work was catalyzed by the synergy between NCSWCs and TBHP. Furthermore, since different types of the doped N atoms have a distinct influence on the catalytic performance of the carbon-based catalysts, NCSWCs with different contents of graphitic and pyridinic N species, such as NCSWC-4-800-M, NCSWC-4-600, NCSWC-4-950, and NCSWC-4-800, were used as the catalysts for this reaction to identify the active sites.[9,10,24] FFCA yield is linearly proportional to the content of graphitic nitrogen species in the order of NCSWC-4-800-M, NCSWC-4-600, NCSWC-4-950, and NCSWC-4-800 in Fig. S9 (ESI†), while there is no correlation between FFCA yield and the content of pyridinic N species. Since the textural properties and morphology of these NCSWCs are similar as shown in Table S2 (ESI†), it can be concluded that the graphitic nitrogen species play a vital role in NCSWCs for HMF oxidation to FFCA. In addition, NMC-800 was also prepared as the reference catalyst and used for this reaction under identical conditions. As shown in Table S2, S3 and S10 (ESI†), NMC-800 is a mesoporous material with a high surface area and large mesopore volume and its graphitic N content is 5.96%, which is higher than that in NCSWC-4-950. However, the FFCA yield over NMC-800 is even lower than that over NCSWC-4-800-M. It is suggested that the wrinkled cages in NCSWCs are much more beneficial for HMF oxidation than the common N-doped mesoporous carbon.

We also performed DFT calculations on the reaction pathway of HMF oxidation to FDCA. HMF oxidation is initiated by the cleavage of the O–O bond of TBHP to produce hydroxyl ($^{\bullet}OH$) and *tert*-butoxy ($(H_3C)_3CO^{\bullet}$) radicals.[25] However, it is found that the $^{\bullet}OH$ radicals can react with TBHP to form $^{\bullet}OOH$ radicals, which are more preferred to be adsorbed on carbon atoms adjacent to the graphitic N atoms of NCSWCs, as shown in Fig. 2. Since $^{\bullet}OOH$ radicals are not stable when HMF molecules are approaching to NCSWCs, the $^{\bullet}OOH$ radical

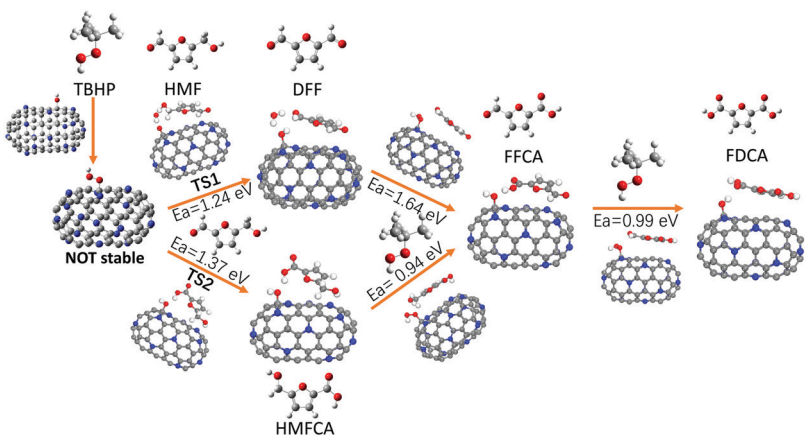

Fig. 2 DFT calculations on the reaction pathway of HMF oxidation to FDCA over NCSWC-4-800 under base-free conditions by using TBHP as the oxidant.

cleaves into •O and •OH radicals adsorbing on carbon atoms adjacent to the graphitic N atoms. The •OH radicals on NCSWCs oxidize the –OH group of the HMF molecule to form C═O and H_2O, while the •O radicals attack the $–CH_2–$ to produce ═CH– and •OH radicals, and then DFF is obtained in the reaction pathway of TS1. Alternatively, the •O radicals alone attack the –HC═O to form HMFCA in the reaction pathway of TS2. However, the energy barrier (E_a) of TS1 is 1.24 eV, lower than that of TS2, indicating that the reaction pathway TS1 was kinetically favoured. Our experimental results also confirmed that the reaction pathway for HMF oxidation was HMF-DFF-FFCA because the yield of HMFCA was very low. Subsequently, the •O radicals adsorbed on carbon atoms adjacent to the graphitic N atoms sequentially oxidize DFF to FFCA, then FDCA. However, if the TBHP/HMF molar ratio is lower than 4, then not enough radicals on NCSWCs oxidize the FFCA to FDCA; if the TBHP/HMF molar ratio is larger than 4, then NCSWCs do not have enough sites to host the •O and •OH radicals, and the undesired products will be produced. Finally, the leaving •OH radicals are allowed for the propagation of the radical reaction in each step until TBHP was completely consumed or reacted with $•C(CH_3)_3$ to form tertiary butyl alcohol.

The results in Fig. S11 (ESI†) show that the HMF conversion and FFCA selectivity remained almost unchanged during 5 catalytic runs, suggesting that NCSWC-4-800 possessed excellent catalytic stability in this reaction. Compared with an N-doped nanoporous graphitic carbon catalyst for HMF oxidation to FDCA under basic conditions reported earlier,[14] where the FDCA yield dropped from 80% to 70% after 4 catalytic runs, the much higher stability of NCSWC-4-800 further implied that graphitic N species are not the active site to generate the oxygen radicals for oxidation, because they are likely to change to the less active oxidized ones, causing the catalyst deactivation during the oxidation reaction.[9]

In summary, NCSWCs were prepared using DFNS as the hard templates through the hydrothermal carbonization combined with the pyrolysis with DABT, followed by silica etching. Among NCSWCs, NCSWC-4-800 exhibited the best catalytic activity with 92.3% HMF conversion and 90.5% FFCA selectivity, which was attributed to its high content of the graphitic nitrogen and largest mesopore and macropore volumes derived from its unique wrinkled cages. When NCSWC-4-800 was compared with the reported metal based catalysts for HMF oxidation to FFCA under base-free conditions (in Table S5, ESI†), although the FFCA yield was comparable with the best reported catalysts, NCSWC-4-800 showed much better catalytic stability. In addition, it was found that HMF oxidation was catalyzed by the synergy between NCSWCs and TBHP and their catalytic activities were linearly correlated with the contents of the graphitic N species in NCSWCs.

JZ and HT gratefully acknowledge the financial support from the research fund (518047 and 519015) from Guangdong University of Petrochemical Technology and the Natural Science Foundation of Guangdong Province (2018A030307053), China. VP acknowledges the department of atomic energy (DAE), government of India (R&D-TFR-RTI4003) for funding.

Conflicts of interest

There are no conflicts to declare.

Notes and references

1 P. V. Rathod and V. H. Jadhav, *ACS Sustainable Chem. Eng.*, 2018, **6**, 5766–5771.
2 K. Gupta, R. K. Rai and S. K. Singh, *ChemCatChem*, 2018, **10**, 2326–2349.
3 P. Paland and S. Saravanamurugan, *ChemSusChem*, 2019, **12**, 145–163.
4 M. Ventura, M. Aresta and A. Dibenedetto, *ChemSusChem*, 2016, **9**, 1096–1100.
5 M. Ventura, F. Lobefaro, E. Giglio, M. Distaso, F. Nocito and A. Dibenedetto, *ChemSusChem*, 2018, **11**, 1305–1315.
6 A. Buonerba, S. Impemba, A. D. Litta, C. Capacchione, S. Milione and A. Grassi, *ChemSusChem*, 2018, **11**, 3139–3149.
7 P. Pal, S. Kumar, M. M. Devi and S. Saravanamurugan, *J. Supercrit. Fluids*, 2020, **160**, 104812.
8 K. Afroz, M. Ntambwe and N. Nuraje, *Inorg. Chem.*, 2020, **59**, 13335–13342.
9 H. Watanabe, S. Asano, S. I. Fujita, H. Yoshida and M. Arai, *ACS Catal.*, 2015, **5**, 2886–2894.
10 Y. Lin and D. S. Su, *ACS Nano*, 2014, **8**, 7823–7833.
11 Y. Cao, H. Yu, F. Peng and H. Wang, *ACS Catal.*, 2014, **4**, 1617–1625.
12 W. Liu, C. Wang, F. Herold, B. J. Etzold, D. S. Su and W. Qi, *Appl. Catal., B*, 2019, **258**, 117982.
13 W. Xiong, Z. Wang, S. He, F. Hao, Y. Yang, Y. Lv, W. Zhang, P. Liu and H. Luo, *Appl. Catal., B*, 2020, **260**, 118105.
14 C. V. Nguyen, Y. Liao, T. Kang, J. E. Chen, T. Yoshikawa, Y. Nakasaka, T. Masuda and K. C. W. Wu, *Green Chem.*, 2016, **18**, 5957–5961.
15 Y. S. Ren, Z. L. Yuan, K. L. Lv, J. Sun, Z. H. Zhang and Q. Chi, *Green Chem.*, 2018, **20**, 4946–4956.
16 M. Xu, Q. Yu, Z. H. Liu, J. S. Lv, S. T. Lian, B. Hu, L. Q. Mai and L. Zhou, *Nanoscale*, 2018, **10**, 21604–21616.
17 H. J. Tian, T. Y. Wang, F. Zhang, S. Q. Zhao, S. Wan, F. R. He and G. X. Wang, *J. Mater. Chem. A*, 2018, **6**, 12816–12841.
18 B. Singh, A. Maity and V. Polshettiwar, *ChemistrySelect*, 2018, **3**, 10684–10688.
19 V. Polshettiwar, D. Cha, X. Zhang and J. M. Basset, *Angew. Chem., Int. Ed.*, 2010, **49**, 9652–9656.
20 A. Maity, R. Belgamwar and V. Polshettiwar, *Nat. Protoc.*, 2019, **14**, 2177–2204.
21 Z. L. Li, J. L. Li, J. H. Liu, Z. L. Zhao, C. G. Xia and F. W. Li, *ChemCatChem*, 2014, **6**, 1333–1339.
22 J. P. S. Sousa, M. F. R. Pereira and J. L. Figueiredo, *Catal. Today*, 2011, **176**, 383–387.
23 T. Zhan, W. B. Liu, J. J. Teng, C. C. Yue, D. H. Li, S. H. Wang and H. Tan, *Chem. Commun.*, 2019, **55**, 2620–2623.
24 J. Zhang, C. Y. Zheng, M. L. Zhang, Y. J. Qiu, Q. Xu, W. C. Cheong, W. X. Chen, L. R. Zheng, L. Gu, Z. P. Hu, D. S. Wang and Y. D. Li, *Nano Res.*, 2020, **13**, 3082–3087.
25 H. Q. Fu, K. T. Huang, G. X. Yang, Y. H. Cao, H. J. Wang, F. Peng, Q. Wang and H. Yu, *ACS Catal.*, 2020, **10**, 129–137.

